$CuCo_2O_4$ ORR/OER Bi-Functional Catalyst: Influence of Synthetic Approach on Performance

Alexey Serov, Nalin I. Andersen, Aaron J. Roy, Ivana Matanovic,* Kateryna Artyushkova, and Plamen Atanassov*,z

Department of Chemical and Nuclear Engineering, Center for Emerging Energy Technologies Farris Engineering Center, University of New Mexico, Albuquerque, New Mexico 87131, USA

A series of $CuCo_2O_4$ catalysts were synthesized by pore forming, sol-gel, spray pyrolysis and sacrificial support methods. Catalysts were characterized by XRD, SEM, XPS and BET techniques. The electrochemical activity for the oxygen reduction and oxygen evolution reactions (ORR and OER) was evaluated in alkaline media by RRDE. Density Functional Theory was used to identify two different types of active sites responsible for ORR/OER activity of $CuCo_2O_4$ and it was found that $CuCo_2O_4$ can activate the O-O bond by binding molecular oxygen in bridging positions between Co or Co and Cu atoms. It was found that the sacrificial support method (SSM) catalyst has the highest performance in both ORR and OER and has the highest content of phase-pure $CuCo_2O_4$. It was shown that the presence of CuO significantly decreases the activity in oxygen reduction and oxygen evolution reactions. The half-wave potential ($E_{1/2}$) of $CuCo_2O_4$-SSM was found as 0.8 V, making this material a state-of-the-art, unsupported oxide catalyst.
 [DOI: 10.1149/2.0921504jes]

Manuscript submitted December 3, 2014; revised manuscript received January 28, 2015. Published February 7, 2015.

Development of highly active bi-functional catalysts, in reactions of oxygen reduction/oxygen evolution (ORR/OER), attracts the attention of not only researchers in academia, but also from industrial R&D centers. The industrial interest is apparent by the growing market for supplying pure hydrogen and oxygen for fuel cell back-up power systems in India and Africa. Presently, both fuel cells and electrolyzers utilize a substantial amount of platinum-group metals (PGM), mainly platinum for ORR and IrO_2 for OER. Despite the fact that platinum is the most active catalyst for oxygen reduction, it has a high price; the discovered resources are scarce and major mining facilities are located in politically unstable countries. On the other side, iridium is one of the least abundant elements in the Earth's crust, making its application commercially unviable. The combination of these factors leads to the problem of the incredibly high price of fuel cell stacks and electrolyzers. There is substantial progress in substituting platinum from the cathode side of fuel cell MEAs,[1] while there has been no such breakthrough for electrolyzers reported in open literature.

Secondly, there is a promising application for bi-functional catalysts in metal-air batteries, especially Lithium-air batteries. Li-air batteries should effectively reduce oxygen during the discharge cycle and evolve oxygen during the charge cycle. Highly efficient catalysts for those cycles are precious metal-based materials: Pt, Au, Ag, Pd.[2,3]

Li-air batteries and electrolyzers will be brought into the broad market, where full substitution of precious metal-based catalysts is needed. Promising materials for this purpose are oxides of transition metals. Transition metal oxides, such as MnO_2, were found to be active in the reaction of oxygen reduction in alkaline media, while NiO is very promising in the oxygen evolution reactions. The main drawback of these oxides is their low electric conductivity, which results in a drop of activity in the electrocatalytic reactions. It is common practice to increase this conductivity by adding carbons to the active materials.[4,5] This approach can be applied to ORR catalysts; however, OER catalysts will have a severe decrease in activity during the oxygen evolution reaction due to the degradation of the carbon supports. From this point of view, for the creation of active and durable bi-functional catalysts, only unsupported materials can be used. Mixed oxides, or compounds such as spinels, perovskites and delafosites possess high electrical conductivity and can be used without the addition of carbon.[6–16]

Herein, we report a systematic study on the influences of the preparation method for the catalyst's morphology, conductivity, phase purity and electrochemical performance of $CuCo_2O_4$ spinels. Four synthetic methods were selected: pore-forming, sol-gel, spray pyrolysis and the sacrificial support method.[17–27] As-prepared materials were tested in ORR/OER reactions and show promising performance, which allows for using them as highly active bi-functional catalysts.

Details on the characterization methods can be found in the Supporting Information. Catalytic activity depends on the intrinsic activity of the material, the number of active sites participating in the desirable reactions, and the accessibility of those active sites to the fuel. The last factor is mainly determined by the morphology of the catalyst; therefore, the design of experiments should be focused on the preparation of catalysts with high surface area. Synthesis of phase-pure spinels by decomposing simple nitrates requires temperatures higher than 700°C and the durations of calcinations >24 h. Such harsh conditions result in sintering the material, increasing its particle size and decreasing its surface area to values below 1 $m^2\ g^{-1}$.

Catalysts Synthesis

Preparation of $CuCo_2O_4$ catalyst by pore-forming (PF) method.— First, the calculated amounts of $Cu(NO_3)_2{*}xH_2O$ and $Co(NO_3)_2{*}6H_2O$ (Sigma-Aldrich) were dissolved in 50 mL of DI water. Then, 2g of urea and 2g sucrose (pore forming agents) in 25 mL of water were added to the nitrates solution. The mixture was allowed to dry in an ultrasound bath overnight at T = 40°C. The dry, solid material was ground with mortar and pestle. The mixture of nitrates and pore-forming agents was loaded in a tube furnace and heat-treated in a N_2 atmosphere: flow rate 100 ccm, T = 450°C, t = 1 h. After heat-treatment, the black powder was ground with mortar and pestle followed by calcinations in air at T = 550°C for 3 h. As-prepared powder was used for physico-chemical and electrochemical characterizations.

Preparation of $CuCo_2O_4$ catalyst by sol-gel (SG) method.— First, the calculated amounts of $Cu(NO_3)_2{*}xH_2O$ and $Co(NO_3)_2{*}6H_2O$ (Sigma-Aldrich) were dissolved in 150 mL of DI water. Then, 10 g of NH_4HCO_3 in 125 mL of water was added drop-wise into the nitrates solution. The sol-like colloidal solution was dried in an oven overnight at T = 85°C. The dry, solid material was ground with mortar and pestle. The mixture of hydroxides was calcined in air at T = 550°C for 3 h. As-prepared powder was used for physico-chemical and electrochemical characterizations.

Preparation of $CuCo_2O_4$ catalyst by spray-pyrolysis (SP) method.— First, the calculated amounts of $Cu(NO_3)_2{*}xH_2O$ and $Co(NO_3)_2{*}6H_2O$ (Sigma-Aldrich) were dissolved in 100 mL of DI water. The solution of nitrates was atomized by means of an

*Electrochemical Society Active Member.
zE-mail: plamen@unm.edu

ultrasound bath and aerosol particles were transported in N_2 gas through a preheated furnace, flow rate 1 L min^{-1}, T = 350°C. Dry, solid material was collected on the Teflon filter at the cold end of furnace. The mixture of oxides was calcined in air at T = 550°C for 3 h. As-prepared powder was used for physico-chemical and electrochemical characterizations.

Preparation of $CuCo_2O_4$ catalyst by SSM method.— First, a known amount of silica (Cab-O-Sil EH-5, surface area: ~400 m^2 g^{-1}) was dispersed in water with an ultrasonic probe. Then, the calculated amounts of $Cu(NO_3)_2{*}xH_2O$ and $Co(NO_3)_2{*}6H_2O$ (Sigma-Aldrich) were added to the silica colloidal suspension. Total loading of metals on silica was calculated to be 17 wt%. Silica and precursors mixture was allowed to dry in an oven overnight at T = 85°C. The dry mixture of silica and nitrates was calcined in air at T = 550°C for 3 h. The silica support was etched by means of 7 M KOH overnight. The obtained wet powder was washed with DI water until a neutral pH was achieved. After drying at T = 85°C, the powder was used for physico-chemical and electrochemical characterizations. In order to compare activity of $CuCo_2O_4$ with CuO the copper oxide was synthesized by the same SSM at the same condition excluding cobalt nitrate addition.

Results and Discussion

In the present work, four alternative synthetic methods were chosen to decrease the synthesis temperatures and times for heat-treatment. The method based on the usage of pore-forming agents (PF) utilizes an idea that during the first heat-treatment in inert atmosphere, several chemical processes will occur: metal nitrates will be decomposed to oxides, decomposition of urea will lead to the release of gaseous products creating pores and channels, and sucrose will be turned into high surface area carbon. During the second heat-treatment of the composite material in air, the carbon will be burned out preventing oxides from agglomerating. The sol-gel (SG) method provides formation of colloidal sols of both precursors pre-mixed on a molecular level, and during the gelation step, hydrated oxides of copper and cobalt will stay at close proximity to one other. The spray-pyrolysis (SP) method results in the formation of relatively large spherical particles, which consists of smaller nanoparticles of oxides. During post-treatment calcinations, such structures are extremely stable and prevent the material from sintering. As it has been shown from our group, the sacrificial support method (SSM) is a powerful tool for the preparation of cathode materials, anode materials and CNTs.[17–27] High surface areas of the final catalyst are a result of removing the sacrificial support, which can be controlled by the selection of silica with different particle sizes and surface areas.

XRD analyses of the four samples show that the $CuCo_2O_4$ made by SSM was a phase-pure spinel (~96 wt%), despite the usage of a significantly lower temperature and calcination duration during synthesis (Figure 1, bottom). This can be explained by homogeneous coverage of the precursors on the surface of mono-dispersed silica particles. Materials made by pore-forming and spray pyrolysis methods had a similar XRD pattern with spinel as a predominant phase (more than 70 wt%) and copper oxide as a side phase.

In the case of $CuCo_2O_4$ made by the sol-gel method, the main phase was CuO (>60 wt%). This phase ratio was formed due to the difference in sol formation for cobalt and copper nitrates. Cobalt nitrate reacts with NH_4HCO_3, forming a colloid nickel hydroxide sol, while copper nitrate forms soluble complexes and malachite-like compounds. In order to use the sol-gel method for making a phase pure $CuCo_2O_4$ spinel, another solation agent should be selected.

The morphology of the four compounds was characterized by SEM imaging (Figure 2). It was observed that the pore-forming method results in the formation of material with uniformly distributed nanoparticles, which were closely attached to each other without forming a porous structure. The $CuCo_2O_4$ material made by the sol-gel method has substantial phase separation with hexagon-shaped particles and particles with irregular structure, which is in good correlation with the XRD analysis where two phases of spinel and CuO was observed.

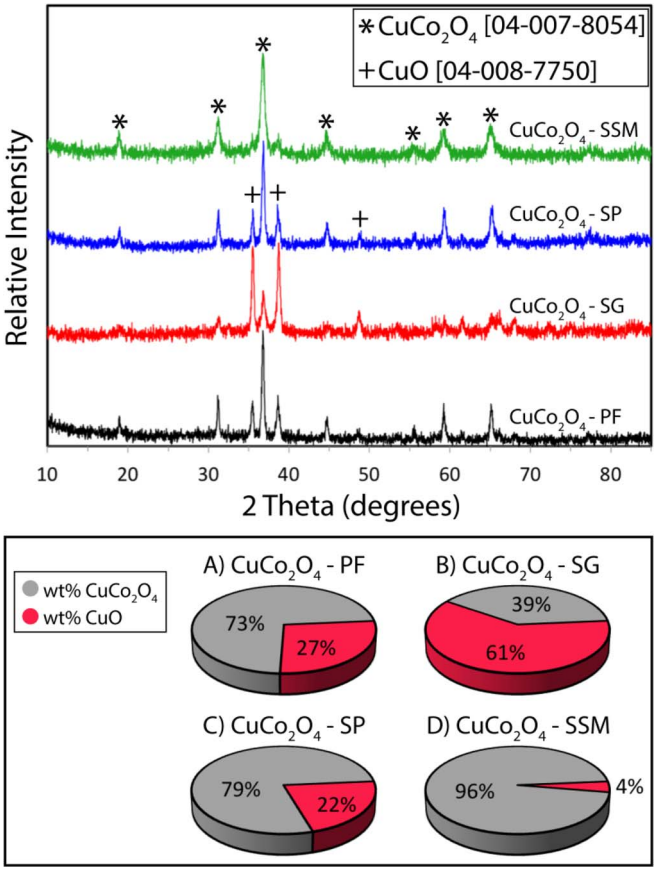

Figure 1. XRD data (top) and weight percentage ratios (bottom) of $CuO:CuCo_2O_4$ for catalysts prepared by a) pore-forming method (PF), b) sol-gel method (SG), c) spray pyrolysis (SP) and d) sacrificial support method (SSM). Condition: T = 550°C, t = 3 h.

There is a presence of large 50–75 nm pores in this material. As it was expected, the spray pyrolysis method resulted in the synthesis of spherical particles in the range of 1–2 μm.[23] It can be seen in Figure 2c that whole spheres are hollow with wall thicknesses ~100–200 nm. Surprisingly, the sacrificial support method produced spinels with spherical morphology (Figure 2d). Up to our best knowledge, this is the first observation that when starting from irregularly fumed silica

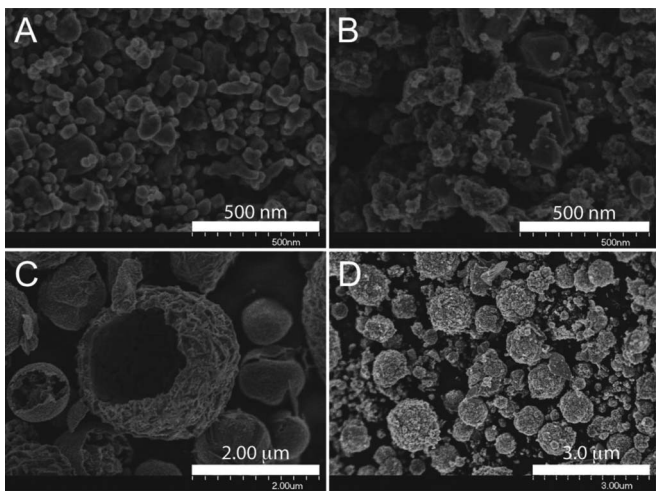

Figure 2. SEM images of $CuCo_2O_4$ catalysts prepared by a) pore-forming method, b) sol-gel method, c) spray pyrolysis and d) sacrificial support method.

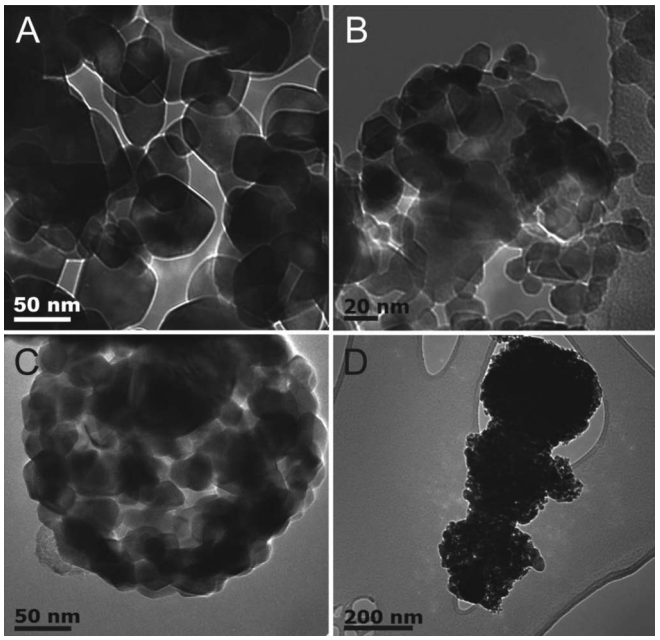

Figure 3. TEM images of $CuCo_2O_4$ catalysts prepared by a) pore-forming method, b) sol-gel method, c) spray pyrolysis and d) sacrificial support method.

as a sacrificial support, one can synthesize hierarchically structured oxide materials.

Low magnification TEM images of prepared spinels are shown in Figure 3. Particle sizes of the materials prepared by PF and SG methods were in good correlation with those observed by SEM. Substantial differences in particle size for the SG method confirms the existence of two phases (Figure 3b). It is clear from Figure 3c that spheres of the spinel made by the SP method consisted of 20–25 nm particles. Figure 3d represents spherical 3D structured particles with an open frame structure of $CuCo_2O_4$ synthesized by SSM. Low magnification TEM data confirmed the average crystallite domain sizes calculated from XRD pattern refinement. The calculated domain size for $CuCo_2O_4$ in pore forming, sol-gel, spray pyrolysis and sacrificial support catalysts is: 15 nm, 34 nm, 18 nm, and 28 nm, respectively.

High-resolution TEM (HRTEM) images for materials with distinct differences in the spinel to copper oxide weight ratios are shown in Figure 4. Spot diffraction patterns for the $CuCo_2O_4$ catalysts prepared by the sol-gel and sacrificial support method were found to be in agreement with the bulk phases identified by X-ray diffraction. The $CuCo_2O_4$ spinel phase in both catalysts was confirmed to be FCC with a corresponding lattice parameter of 8.1 Å. The CuO phase was not observed by HRTEM in the sample prepared by the SSM method, which is consistent with the composition determined by X-ray diffraction pattern refinement, <5 wt% CuO with the bulk phase consisting of the $CuCo_2O_4$ spinel. Analysis of the spot diffraction patterns for the catalyst prepared by the sol-gel method (Figure 4a lower left) confirm the presence of the monoclinic CuO phase with the corresponding lattice parameters of: a = 4.7 Å, b = 3.4 Å, and c = 5.1 Å. The (002) reflection with a corresponding d-spacing of 2.5 Å is that of CuO. The other d-spacings in Figure 4 show the $CuCo_2O_4$ spinel (111) reflection. It was confirmed that $CuCo_2O_4$-SG contained both spinels and CuO phases, while $CuCo_2O_4$-SSM consists mainly of spinel.

Detailed XPS analysis of all synthesized catalysts was performed, where Figure 5 shows Co 2p and Figure S2 shows Cu 2p high resolution spectra. It has been shown that satellite structures in Co 2p, and not the absolute binding energies and ratios of intensities of peaks, are better able to distinguish between CoO and cobalt-containing spinel with octahedrally coordinated Co^{2+}. The binding energy of satellite due to pure spinel is higher than that due to CoO. Hence, there is an

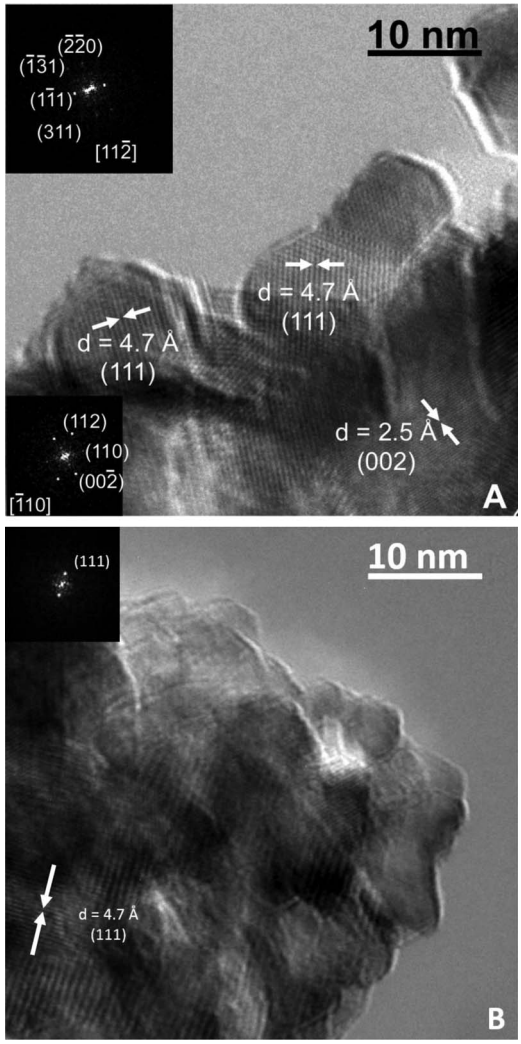

Figure 4. High resolution TEM images of $CuCo_2O_4$ catalysts with weight percentage ratios ($CuCo_2O_4$:CuO) prepared by a) sol-gel method (39:61) and b) sacrificial support method (96:4).

expected correlation between the purity of the spinel phase and the binding energy positon of the satellite peak in the Co 2p spectrum. Therefore, we did not deconvolve the high resolution Co 2p spectra, but focused on the position of the satellite peak as shown in Figure 5. The change in the octahedral environment of Co in the spinel will lead to a decrease in binding energy of the satellite peak and a decrease in its intensity. As seen from the Co 2p spectra, the position of the satellite signature of the spinel at 798.8 eV for the SSM sample is shifted to lower values, up to 789.1 eV, for other samples which have a larger amount of CuO with respect to a pure spinel. Cu 2p spectra has been deconvoluted into several components due to Cu oxides (932–935 eV) and due to spinel at 931.2 eV. From the position of the satellite peak in Co 2p spectra and the relative amount of the peak due to the spinel in the Cu 2p spectra, the SSM sample has the purest spinel phase out of the four samples synthesized.

All materials have disordered phases, such as oxides and a second phase of pure spinel. High resolution XPS analysis provides two metrics of spinel purity within the synthesized materials, i.e. the binding energy of satellite in the Co 2p spectra and relative abundance of the spinel peak in the Cu 2p spectra. Correlations between the BE position of satellite due to spinel in the Co 2p spectra versus the relative amount of peak due to spinel in the Cu 2p spectra indicates that these parameters indeed represent the purity of the spinel phase which is highest for the SSM sample.

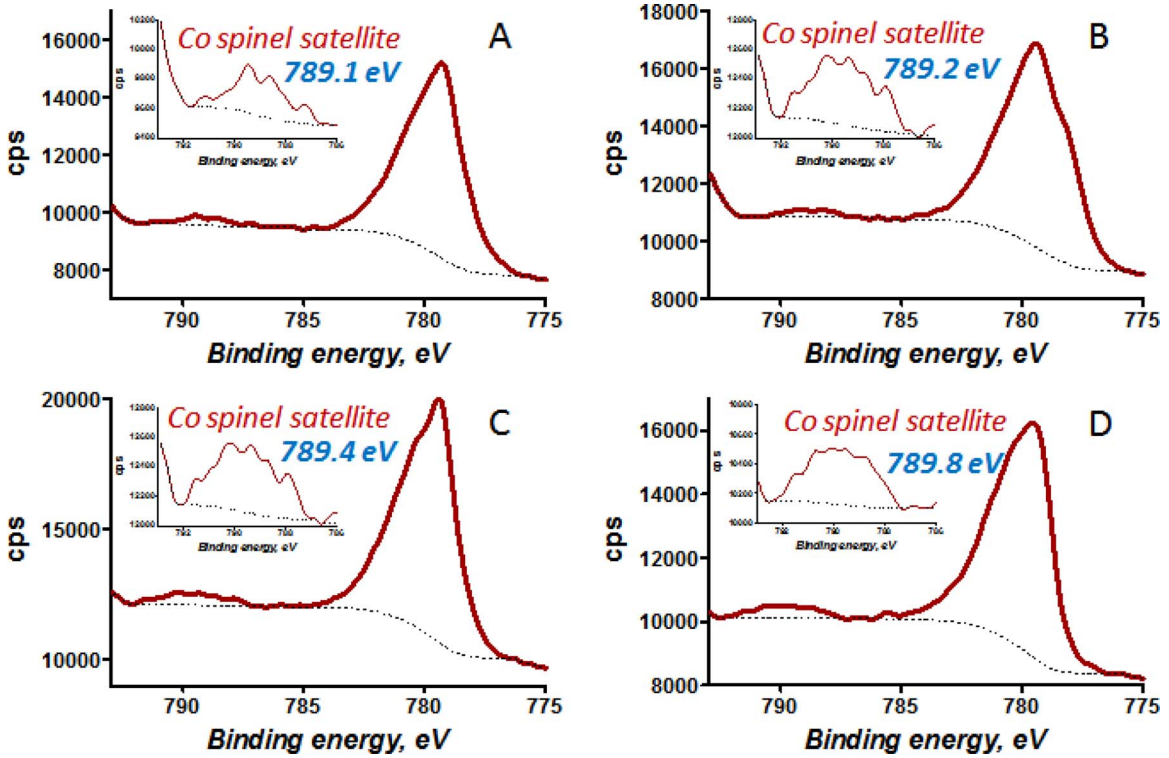

Figure 5. High resolution Co 2p spectra for a) pore-forming method (PF), b) sol-gel method, c) spray pyrolysis (SP) and d) sacrificial support method (SSM). Inset shows a zoomed in satellite structure due to spinel and its position for each of the spectra.

The morphological analysis was in good correlation with surface areas (SA) measured for all four materials by BET. It was found that the SA decreases in the following sequence: $CuCo_2O_4$-SSM > $CuCo_2O_4$-SG > $CuCo_2O_4$-SP > $CuCo_2O_4$-PF, with the values: 42 > 23 > 10 > 9 $m^2\ g^{-1}$, respectively. As it was mentioned earlier, the SA of phase pure spinels synthesized at T > 700°C do not exceed 1 $m^2\ g^{-1}$. It is clear that using the sacrificial support method, phase pure copper-cobalt spinels with a surface area close to 50 $m^2\ g^{-1}$ can be prepared.

The electrochemical data on oxygen reduction measured by the RRDE technique is shown in Figure 6A. It should be noticed that prior to recording the cyclic voltammograms, the working electrode was scanned in the potential window of interest until it reached a steady-state. In order to establish reproducibility of the performed experiments, all measurements were repeated three times. The most active catalyst for ORR was found to be $CuCo_2O_4$-SSM with an impressive half-wave potential ($E_{1/2}$) of 0.8 V, which is just 50 mV below the half-wave potential of the performance of platinum as it was shown by Mayrhofer et al.[28] Such a high-value for an unsupported, spinel material places it among state-of-the-art ORR catalysts.

The performances of the SP, SG and PF materials were similar to each other, with substantially worse limiting currents compared to the SSM sample. The catalyst with the lowest performance was found to be the sol-gel catalyst, and it should be mentioned that this $CuCo_2O_4$-SG catalyst produced the largest amount of H_2O_2. Such behavior indicates a preferable $2e^-$ mechanism of O_2 electroreduction to hydrogen peroxide. Electrochemical performance in the oxygen evolution reaction shows the same trend (Figure 6B). The catalyst made by the sacrificial support method possesses the highest performance with an onset potential of 1.51 V, while the sol-gel prepared sample has the lowest activity.

From Figure 1, the SSM sample is almost phase pure, while the SG material consists mainly of CuO. In order to correlate phase-purity and the presence of CuO, two hypotheses were suggested: CuO has an intrinsically low ORR and OER activity or that CuO has low conductivity, which decreases the overall conductivity of the SG catalyst.

In order to test these hypotheses, additional experiments were performed. A fifth catalyst was synthesized, CuO-SSM, following the same procedures as the CuCo2O4-SSM catalyst, but without the addition of $Co(NO_3)_2$. The catalyst morphology was found to be similar to $CuCo_2O_4$-SSM material (not shown). A resistivity (ρ) measurement of pressed pellets of $CuCo_2O_4$-SSM shows this material is extremely conductive with $\rho < 1\ \Omega$ m, while the CuO-SSM material has $\rho = 210\ k\Omega$ m. The large difference in conductivity plays a crucial role in the performance of the electrochemical reactions. The determination of intrinsic ORR/OER catalytic activity of CuO-SSM was measured with the same conditions as for the spinels. Results of the ORR and OER performance of CuO-SSM in comparison with $CuCo_2O_4$-SG sample are shown in Figure S3. As one can see, the limiting current from the ring and disk for CuO-SSM is the same, proving a pure $2e^-$ process, which explains the highest H_2O_2 yield for the SG spinel. OER activity of CuO-SSM was significantly lower when compared to the copper-cobalt spinel prepared by the sol-gel method.

These collective results indicate that the addition of copper oxide to the phase pure $CuCo_2O_4$ spinel has a dual mechanism: it significantly drops the electric conductivity and also decreases the ORR/OER activity due to the intrinsically low activity of CuO-SSM in both reactions. In order to design a highly conductive material and active material, phase pure copper-cobalt spinel has to be prepared. It also should be mentioned that there is about 700 mV overpotential between ORR and OER. As discussed later, Density Functional Theory calculations confirm that this phenomenon may be explained by the assumption that oxygen reduction and oxygen evolution occur on different active sites.

In order to gain better understanding of the differences in the reactivity of CuO-SSM and $CuCo_2O_4$ phases, models were made to show the number of possible active centers on CuO(111) and $CuCo_2O_4$(111) surfaces (Figure 7). Density Functional

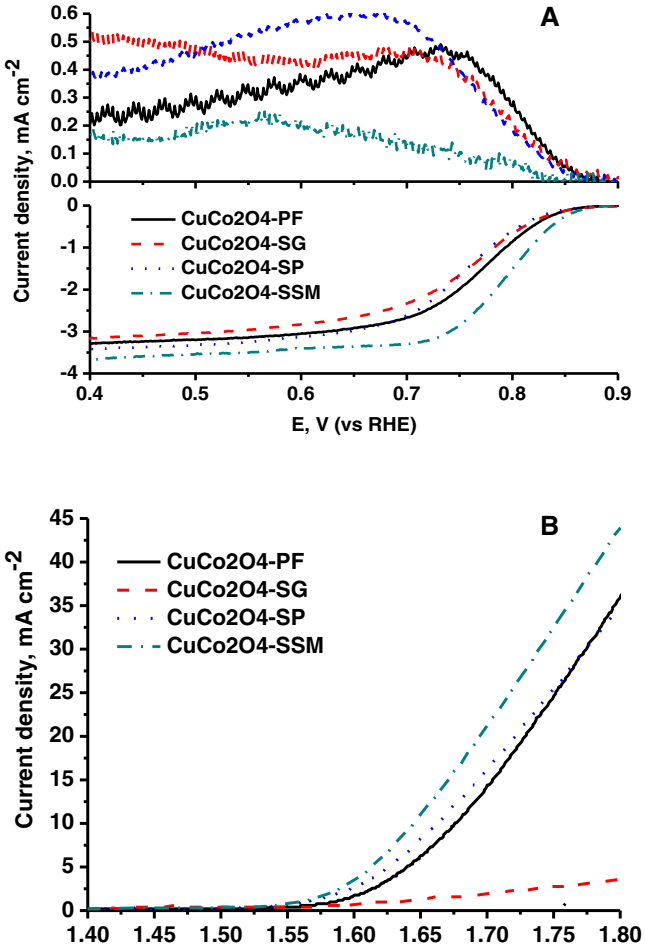

Figure 6. Electrochemical data on $CuCo_2O_4$ catalysts: a) RRDE in oxygen reduction, b) RDE in oxygen evolution. Conditions: catalyst loading -200 μg cm^{-2}, 1 M KOH, 1600 RPM, 10 mV s^{-1}, ring material: Pt, collection efficiency: 37%, potential on Pt_{ring}: 1.5 V. Data are not iR-corrected.

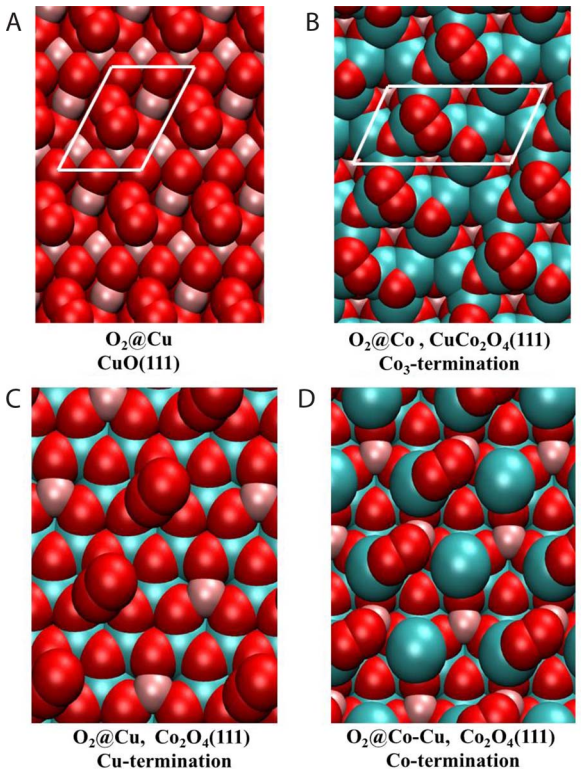

Figure 7. Density functional study of oxygen adsorption on different sites of CuO(111) and several different terminations of $CuCo_2O_4$(111) surfaces. Red – O, blue- Co, and pink- Cu atoms.

Theory (DFT) was used to obtain oxygen binding energies and structural geometries (details of the calculations are given in Supporting Information).

Catalysis of the ORR can be correlated with the adsorption affinity of oxygen,[29] and based on DFT results, $CuCo_2O_4$ has several active centers that have favorable interaction with molecular oxygen: Co atoms on Co-terminated $CuCo_2O_4$(111) and Co/Cu atoms on Co3-terminated $CuCo_2O_4$(111) surface with oxygen adsorption energies of -0.98 eV and -2.56 eV, respectively (Table I).[29]

Moreover, on both of these catalytic sites, the oxygen molecule adsorbs in a bridge position between Co or Co and Cu atoms with an activated oxygen-oxygen bond of 1.46 Å and 1.36 Å, which also indicates a preference of the $CuCo_2O_4$ phase for dissociative 4e$^-$ mechanism of ORR with minimal production of H_2O_2. Different types of active centers are responsible for high OER activity of the $CuCo_2O_4$ phase, which confirms our assumption that ORR and OER occur at different catalytic sites. Cu centers on Cu-terminated $CuCo_2O_4$(111) have low affinity for molecular oxygen, and when compared with other studied sites and their oxygen affinities, these sites are good candidates for OER active centers. The CuO(111) surface has two non-equivalent types of Cu atoms per one unit cell, but based on our DFT results, only one type of Cu center, the one with under-coordinated Cu, shows any affinity for molecular oxygen. In addition, there is only one reactive Cu site per surface unit cell of CuO(111) and, thus, we expect this phase to have very low intrinsic activity, as confirmed by the experiments.

We further calculated ORR/OER free energy diagrams for the two sites that are proposed to have high ORR or OER activity, namely, Co_3- and Cu-terminated $CuCo_2O_4$(111) surfaces. The details of the calculation are given in the supporting information and the final results are given in Figure 8.

Our results show that OOH species are not stable on the Co_3-terminated $CuCo_2O_4$(111) surface and dissociate on OH and O species. Thus, we considered only a dissociative mechanism on the Co_3-terminated $CuCo_2O_4$(111) surface. Based on the free energy diagram for the oxygen reduction reaction on the Co_3-terminated $CuCo_2O_4$(111) surface (Figure 8), at potentials between 0.0 V and 0.70 V, all the steps in the oxygen reduction mechanism on the Co_3-terminated $CuCo_2O_4$(111) surface are exothermic, and oxygen reduction should run at potentials between 0.0 and 0.70 V. At potentials between 0.0 and 0.23 V, all the steps in the oxygen reduction mechanism on the Cu-terminated $CuCo_2O_4$(111) surface are exothermic, and for the potentials beyond 1.80 V all oxygen evolution steps on the Cu-terminated $CuCo_2O_4$(111) surface become exothermic (Figure 8).

Table I. Adsorption energies of molecular oxygen on CuO(111) (Figure 7a) and $CuCo_2O_4$(111) surfaces with Co_3-termination (Figure 7b), Cu-termination (Figure 7c), and Co-termination (Figure 7d) as calculated using GGA-PW91.

Surface	Co site Oxygen binding energy/eV	Cu site Oxygen binding energy/eV
CuO(111)		−0.48
$CuCo_2O_4$ (111), Co_3-termination	−0.98	
$CuCo_2O_4$ (111), Cu-termination		−0.21
$CuCo_2O_4$ (111), Co-termination	−2.56	−2.56

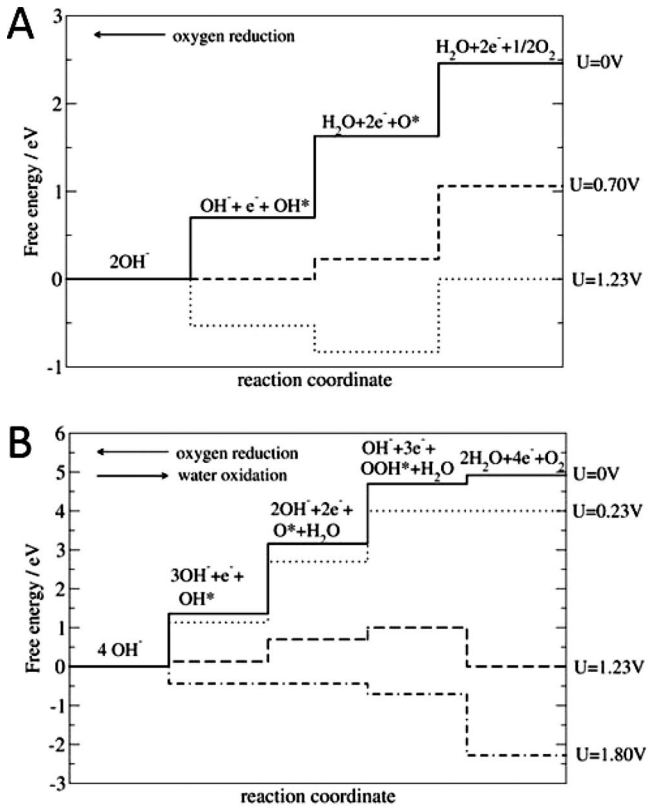

Figure 8. a) Free energy diagram for the dissociative mechanism of oxygen reduction on the Co_3- terminated $CuCo_2O_4(111)$ surface in alkaline media and b) Free energy diagram for the associative mechanism of oxygen reduction/water oxidation on the Cu-terminated $CuCo_2O_4(111)$ surface in alkaline media. The variation of the free energy with respect to the potential is obtained by varying the term e*U* in the free energy per electron transferred to the electrode.

Consequently, the Cu-terminated $CuCo_2O_4(111)$ surface has a very high overpotential for the ORR reaction, but is active for OER at potentials higher than 1.80 V. Calculated values are in good agreement with the experimentally determined half-wave potentials for ORR of 0.80 V and the OER onset potential of 1.51 V. DFT determined overpotentials for ORR and OER are slightly overestimated, probably due to the fact that PW91 functional overestimates binding of OH species.[30]

Conclusions

A systematic study on the influences of the preparation methods on electrocatalytic performance in ORR and OER of $CuCo_2O_4$ spinels was performed in the present study. Four different synthetic approaches were selected in order to make materials with high surface area and porous structure: pore-forming, sol-gel, spray pyrolysis and sacrificial support methods. It was found that even at low temperature, the SSM allows for the synthesis of a phase-pure spinel, while other methods result in a mixture of $CuCo_2O_4$ and CuO-SSM phases. The sol-gel method produces material with the highest amount of copper oxide.

Electrochemical data reveals high activity for the $CuCo_2O_4$-SSM in ORR with $E_{1/2} = 0.8$ V; it can be emphasized that for self-supported oxide materials, such performance is 100 mV below Pt/C and this catalyst is state-of-the-art in its class. The same material shows the highest activity in OER when compared to the other preparation methods. In both reactions, the $CuCo_2O_4$-SG was found to have the lowest performance. In order to understand that phenomenon, two hypotheses were formulated and experimentally confirmed. It was clearly shown that the presence of CuO in the $CuCo_2O_4$ spinel plays a dual role: decreasing the electrical conductivity and decreasing the activity due to the intrinsic catalytic inertness of CuO in ORR and OER.

The SSM is a powerful tool, and can be adopted for the preparation of spinels with high surface area, porosity and hierarchically structured 3D morphology. Phase-pure $CuCo_2O_4$ made by the sacrificial support method was found to be a promising candidate to substitute PGM materials in bi-functional energy conversion applications.

Acknowledgment

Computational work was performed using computational resources/license agreements of Los Alamos National Laboratory, which is operated by Los Alamos National Security, LLC for the National Nuclear Security Administration of U.S. Department of Energy under contract DE-AC52-06NA25396 and the computational resources of the Environmental Molecular Sciences Laboratory, a national scientific user facility sponsored by the Department of Energy's Office of Biological and Environmental Research and located at Pacific Northwest National Laboratory.

References

1. E. Proietti, F. Jaouen, M. Lefèvre, N. Larouche, J. Tian, J. Herranz, and J. P. Dodelet, *Nat. Comm.*, **2**, 1 (2011).
2. J. Greeley, I. E. L. Stephens, A. S. Bondarenko, T. P. Johansson, H. A. Hansen, T. F. Jaramillo, J. Rossmeisl, I. Chorkendorff, and J. K. Norskov, *Nature Chem.*, **1**, 552 (2009).
3. T. Reier, M. Oezaslan, and P. Strasser, *ACS Catal.*, **2**, 1765 (2012).
4. Y. Liang, Y. Li, H. Wang, J. Zhou, J. Wang, T. Regier, and H. Dai, *Nat. Mater.*, **10**, 780 (2011).
5. L. Wang, X. Zhao, Y. Lu, M. Xu, D. Zhang, R. S. Ruoff, K. J. Stevenson, and J. B. Goodenough, *J. Electrochem. Soc.*, **158**, A1379 (2011).
6. L. Jörissen. *J. Power Sources.* **155**, 23 (2006).
7. Y. Gorlin and T. F. Jaramillo, *J. Am. Chem. Soc.*, **132**, 13612 (2010).
8. G. N. Pirogova, N. M. Panich, R. I. Korosteleva, Y. V. Voronin, and N. N. Popova, *Russ. Chem. Bull. Int. Ed.*, **49**, 1536 (2000).
9. M. Hamdani, R. N. Singh, and P. Chartier, *Int. J. Electrochem. Sci.*, **5**, 556 (2010).
10. C. Jin, F. Lu, X. Cao, Z. Yang, and R. Yang, *J. Mater. Chem. A.*, **1**, 12170 (2013).
11. S. Müller, K. Striebel, and O. Haas, *Electrochim. Acta.*, **39**, 1661 (1994).
12. O. Haas, F. Holzer, S. Müller, J. M. McBreen, X. Q. Yang, X. Sun, and M. Balasubramanian, *Electrochim. Acta.*, **47**, 3211 (2002).
13. X. Wu and K. Scott, *J. Power Sources.*, **206**, 14 (2012).
14. M. Bursell, M. Pirjamali, and Y. Kiros, *Electrochim. Acta.*, **47**, 1651 (2002).
15. C. Jin, X. Cao, L. Zhang, C. Zhang, and R. Yang, *J. Power Sources.*, **241**, 225 (2013).
16. Y. Shimizu, K. Uemura, H. Matsuda, N. Miura, and N. Yamazoe, *J. Electrochem. Soc.*, **137**, 3430 (1990).
17. A. Serov, U. Martinez, A. Falase, and P. Atanassov, *Electrochem. Comm.*, **22**, 193 (2012).
18. S. Pylypenko, O. Mukherjee, T. S. Olson, and P. Atanassov, *Electrochim. Acta.*, **53**, 7875 (2008).
19. M. H. Robson, A. Serov, K. Artyushkova, and P. Atanassov, *Electrochim. Acta.*, **90**, 656 (2013).
20. S. Brocato, A. Serov, and P. Atanassov, *Electrochim. Acta.*, **87**, 361 (2013).
21. N. I. Andersen, A. Serov, and P. Atanassov, *Appl. Catal. B: Environmental*, (2014).
22. A. Serov, M. Padilla, A. J. Roy, P. Atanassov, T. Sakamoto, K. Asazawa, and H. Tanaka, *Angewandte Chemie Int. Ed.* (2014).
23. U. Martinez, A. Serov, and M. Padilla Plamen Atanassov, *ChemSusChem*, (2014).
24. U. Tylus, Q. Jia, K. Strickland, N. Ramaswamy, A. Serov, P. Atanassov, and S. Mukerjee, *J. Phys. Chem. C*, **118**(17) 8999 (2014).
25. A. Serov, U. Martinez, and P. Atanassov, *Electrochem. Comm.*, **34**, 185 (2013).
26. A. Serov, K. Artyushkova, and P. Atanassov, *Adv. Energy Mater.*, **4**, 1301735 (2014). doi: 10.1002/aenm.201301735.
27. A. Serov, A. Aziznia, P. H. Benhangi, K. Artyushkova, P. Atanassov, and E. Gyenge, *J. Mater. Chem. A*, **1**, 14384 (2013).
28. K. J. J. Mayrhofer, G. K. H. Wiberg, and M. Arenzz, *J. Electrochem. Soc.*, **155**, 1 (2008).
29. J. Greeley, I. E. L. Stephens, A. S. Bondarenko, T. P. Johansson, H. A. Hansen, T. F. Jaramillo, J. Rossmeisl, I. Chorkendorff, and J. K. Norskov, *Nature Chemistry*, **1**, 552 (2009).
30. I. Matanović, F. H. Garzon, and N. J. Henson, *J. Phys. Chem. C*, **115**, 10640 (2011).

Journal of The Electrochemical Society, **162** (4) X9-X9 (2015)
0013-4651/2015/162(4)/X9/1/$33.00 © The Electrochemical Society

Erratum: Dynamic Mechanical Analysis of Phase Transformations and Anelastic Relaxation in Stabilized Zirconias [*J. Electrochem. Soc.*, 162, F14 (2015)]

Peipei Gao,[a] Edgar Lara-Curzio,[b] Rosa Trejo,[b] and Miladin Radovic[a,c]

[a]*Department of Mechanical Engineering, Texas A&M University, College Station, Texas 77843-3123, USA*
[b]*Materials Science and Technology Division, Oak Ridge National Laboratory, Oak Ridge, Tennessee 37831, USA*
[c]*Department of Materials Science and Engineering, Texas A&M University, College Station, Texas 77843-3003, USA*

 [DOI: 10.1149/2.0971504jes] Published February 7, 2015.

On page F17, right column, Figure 5 should be

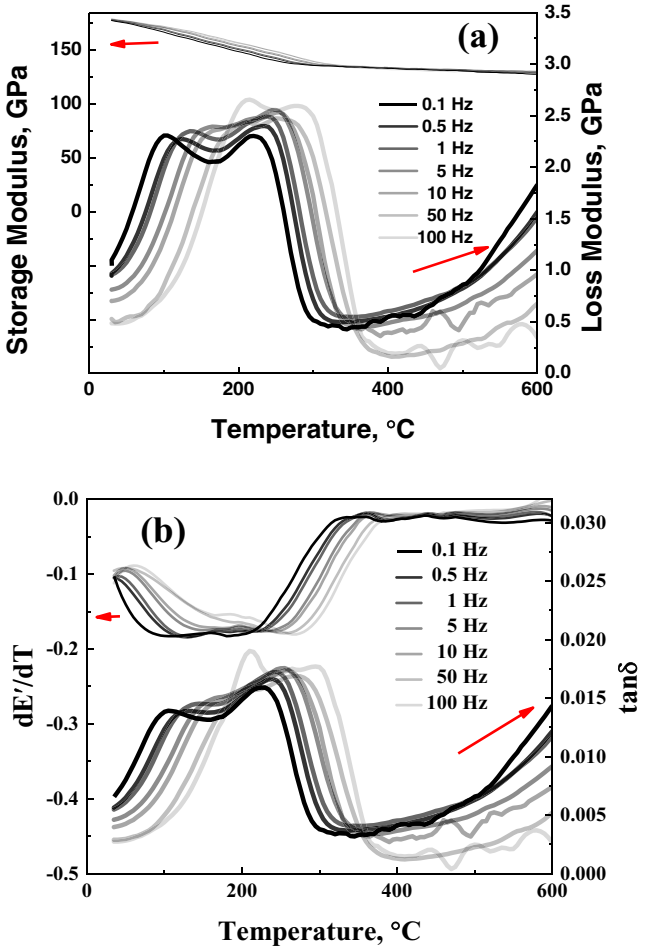

Figure 5. (a) Storage modulus (E') and loss modulus (E''), as well as (b) dE'/dT and tanδ vs. temperature plots for 10 mol% YSZ.

On page F18, right column, Figure 7 should be

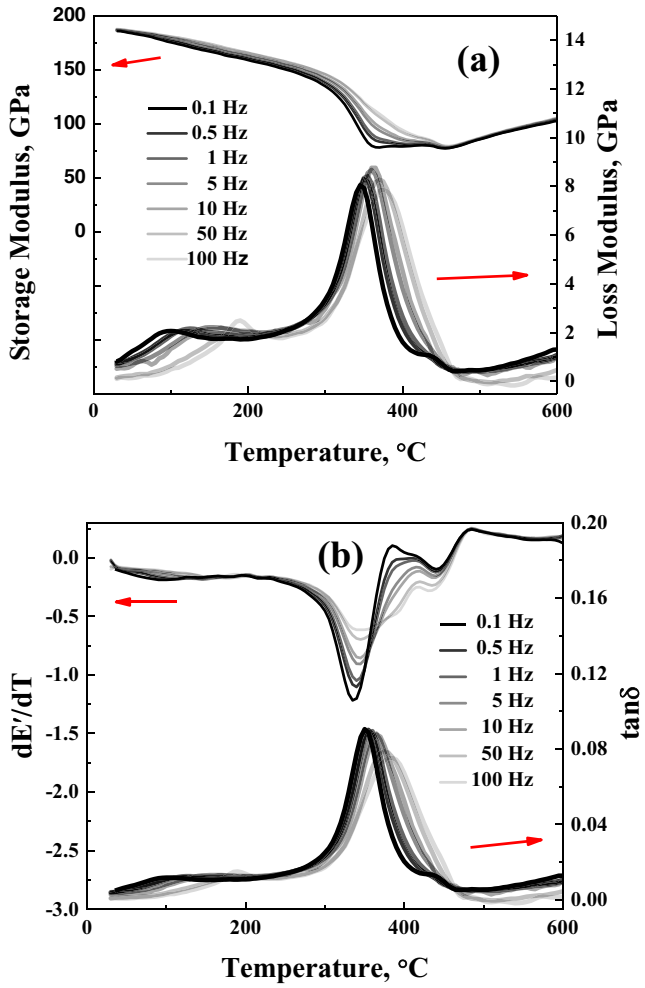

Figure 7. (a) Storage modulus (E') and loss modulus (E''), as well as (b) dE'/dT and tanδ vs. temperature plots for 100% cubic SCSZ.